



Microstructure and properties of cold drawing Cu-2.5% Fe-0.2% Cr and Cu-6% Fe alloys*

Guo-huan BAO¹, Yi CHEN¹, Ji-en MA², You-tong FANG², Liang MENG¹,
 Shu-min ZHAO³, Xin WANG³, Jia-bin LIU^{†‡1}

¹Department of Materials Science and Engineering, Zhejiang University, Hangzhou 310027, China)

²College of Electrical Engineering, Zhejiang University, Hangzhou 310027, China)

³College of Materials and Environmental Engineering, Hangzhou Dianzi University, Hangzhou 310018, China)

[†]E-mail: liujiabin@zju.edu.cn

Received Sept. 22, 2014; Revision accepted Mar. 1, 2015; Crosschecked July 20, 2015

Abstract: High strength and high conductivity Cu-based materials are key requirements in high-speed railway and high-field magnet systems. Cu-Fe alloys represent one of the most promising candidates due to the cheapness of Fe compared to Cu-Ag and Cu-Nb alloys. The high strength of Cu-Fe alloys primarily relies on the high density of the Cu/Fe phase interface, which is controlled by the co-deformation of the Cu matrix and Fe phase. In this study, our main attention was focused on the deformation behavior of the Fe phase using different scales. Cu-2.5% Fe-0.2% Cr (in weight) and Cu-6% Fe alloys were cast, annealed, and cold drawn into wires to investigate their microstructure and properties evolution. Cu-6% Fe contains Cu matrix and Fe, which become the primary particles in the micrometer scale after solution treatment. Cu-2.5% Fe-0.2% Cr contains Cu matrix and Fe precipitate particles in a nanometer scale after solution and aging treatment. The Fe primary particles were elongated and evolved into ribbons in a nanometer scale while the Fe precipitate particles were hardly deformed even at a drawing strain of 6. The reason for the unchanging characteristics of Fe precipitate particles is due to the size effect and incoherent phase interface of Cu matrix and Fe precipitate particles. The strength of both Cu-6% Fe and Cu-2.5% Fe-0.2% Cr alloys increases with the increase in the drawing strain. The electrical resistivity of Cu-6% Fe gradually increases and that of Cu-2.5% Fe-0.2% Cr keeps almost constant with the increase in the drawing strain.

Key words: Copper alloys, Deformation, Microstructure, Strength

doi:10.1631/jzus.A1400285

Document code: A

CLC number: TG146.3

1 Introduction

Cu-based *in situ* filamentary alloys prepared by heavy cold processing, such as using Cu-Nb, Cu-Cr, Cu-Fe, and Cu-Ag, have been studied for decades

due to their high strength and high conductivity (Mattissen *et al.*, 1999; Tian *et al.*, 2011; Jia *et al.*, 2013; Raju *et al.*, 2013; Deng *et al.*, 2014; Pansyrny *et al.*, 2014; Wang *et al.*, 2014). These high strength and high conductivity alloys are expected to be used as conductor materials in high-field magnet and recently developing high-speed railways.

In these alloys, the second elements always have limited solubility in Cu at room temperature. The microstructure of these alloys contains a Cu matrix and second phase. During the cold drawing, both the Cu matrix and second phase are elongated and evolved into filamentary structures at high drawing strains. The density of the phase interface increases

[‡] Corresponding author

* Project supported by the National Natural Science Foundation of China (No. 11202183), the National High-Tech R&D Program (863 Program) of China (No. 2011AA11A101), the Public Projects of Zhejiang Province (No. 2012C31023), and the Zhejiang Provincial Natural Science Foundation of China (No. LQ12B01001)

ORCID: Guo-huan BAO, <http://orcid.org/0000-0003-2155-4961>; Jia-bin LIU, <http://orcid.org/0000-0002-6974-9680>

© Zhejiang University and Springer-Verlag Berlin Heidelberg 2015

as the diameter and interval of the second phase decreases. The strength of the heavy drawn alloys significantly exceeds the predicted strength by the rule of mixture for high drawing strains. The abundant phase interface is thought to play a major role in the strengthening behavior of these alloys. The production of abundant phase interface relies on the co-deformation of the Cu matrix and second phase. Much attention was focused on the deformation behavior of the alloys, especially the second phase, during cold drawing. The co-deformation of Cu-Ag alloys has been well documented in our previous study (Liu *et al.*, 2011a). Since both Cu and Ag phases belong to the face centered cubic (FCC) phase, and they have a cube-on-cube orientation relationship, the two phases could keep an almost synchronous co-deformation during cold drawing. However, the co-deformation of the Cu-body centered cubic (BCC) (Cu-Nb, Cu-Cr, or Cu-Fe) system is very complicated (Spitzig *et al.*, 1987; Biselli and Morris, 1996; Sinclair *et al.*, 1999). The BCC phase has a different dislocation slip system in association with a Cu matrix. Moreover, the BCC phase always has different strain hardening characteristics in association with a Cu matrix. Some general criteria for the co-deformation of FCC-BCC alloys were stated by Sinclair *et al.* (1999), including the resolved shear stress, the angle between the incident and activated systems, and the resulting configuration at the phase interface. The original Nb dendrites in Cu-Nb alloys always have a scale of tens of micrometers (Spitzig *et al.*, 1987). The Nb dendrites gradually evolved into Nb ribbons with a scale of nanometers at high drawing strains. When included in Cu-Cr alloys, original Cr dendrites and Cr-Cu eutectic always have a scale of several micrometers. Both the Cr dendrites and Cr-Cu eutectic gradually evolved into ribbons at high strains with a large scale of nanometers, because Cr appears in two microstructure morphologies (Raabe *et al.*, 2000).

Similar situations occur with the Fe primary dendrites in Cu-Fe alloys (Biselli and Morris, 1994; Xie *et al.*, 2011). In our previous studies, the strain of Fe dendrite linearly increased with an increase in the drawing strain up to 6, and deviated from the linear relationship when the drawing strain was higher than 6 in Cu-12% Fe (in weight) (Lu *et al.*, 2014). The thickness, width, and spacing of Fe ribbons in the filamentary structure exponentially de-

creased with an increase in the drawing strain. The density of the interface between Cu and Fe phases exponentially increased with an increase in the aspect ratio of Fe ribbons. In addition, for the Fe primary dendrites, plenty of Fe precipitate particles were produced in the solution and aging of the Cu-Fe alloys (Monzen and Kita, 2002; Watanabe *et al.*, 2008). These Fe precipitate particles have an initial scale of only several nanometers. Whether the deformation behavior of these nano-particles is the same with that of the micro-dendrites in Cu-Fe alloys still remains unclear. In this study, Cu-2.5% Fe-0.2% Cr and Cu-6% Fe (in weight) alloys were used to prepare Fe nano-particles and Fe micro-dendrites. The deformation behavior between Fe nano-particles and Fe micro-dendrites was compared and analyzed. The evolution of the mechanical and electrical properties of both alloys was investigated based on the microstructure analysis.

2 Materials and methods

Cu-2.5% Fe-0.2% Cr and Cu-6% Fe alloys were melted in a vacuum induction furnace and cast into cylindrical ingots of 22 mm in diameter in a copper mold. According to the Cu-Fe phase diagram, the maximum solubility of Fe in Cu is 4.1% at 1098 °C. In this study, we chose Cu-6% Fe to obtain primary Fe dendrites, and chose Cu-2.5% Fe-0.2% Cr to obtain precipitate Fe particles. Very little Cr addition in Cu-Fe alloys was found to be able to promote the precipitation of Fe and to strengthen the Fe precipitate (Hong and Song, 2001; Song *et al.*, 2001). The Cu-2.5% Fe-0.2% Cr ingots were homogenized at 900 °C for 8 h, and solution treated at 1050 °C for 4 h followed by water quenching, then aged at 700 °C for 33 h. The Cu-6% Fe ingots were homogenized at 900 °C for 8 h, and solution treated at 1050 °C for 4 h followed by water quenching. The surface layer of the ingots was turned off to remove the surface oxides and defects. The ingots were cold worked by rolling and drawing to a drawing strain of $\eta=6.6$, where $\eta=\ln(A_0/A)$, and A_0 and A are the original and final transverse section areas, respectively. No intermediate annealing was applied to the drawn wires.

Ultimate tensile strength was determined at ambient temperature using an electronic tensile testing machine at a strain rate of $2 \times 10^{-3} \text{ s}^{-1}$. Electrical resistivity was measured at room temperature using a standard four-point technique. The microstructure was observed by optical microscopy (OM), scanning electron microscopy (SEM, Hitachi S4800, Japan), and transmission electron microscopy (TEM, FEI F20, USA). TEM observation was carried out in the TEM operating at 200 kV. The TEM samples were prepared by mechanical thinning to about 40 μm and then ion milled at 4 kV with an incidence angle of 8° . The energy-dispersive spectrometer (EDS, Oxford INCA, UK) equipped in F20 was used to perform composition analysis.

3 Results

The microstructure of the solution treated Cu-6% Fe alloy consists of Fe primary particles and Cu grains with an average diameter of 75.7 μm (Fig. 1a). The Fe primary particles with an average diameter of 4.8 μm are dispersed in the Cu grains or near the grain boundaries. The microstructure of aged Cu-2.5% Fe-0.2% Cr alloy consists of Cu grains with an average diameter of 97.3 μm (Fig. 1b). No Fe primary particle was observed in the microstructure of

Cu-2.5% Fe-0.2% Cr, which is different with the microstructure of Cu-6% Fe. TEM results show that there are plenty of Fe-rich precipitate particles with an average diameter of 52.4 nm in the Cu matrix (Fig. 1c). EDS results of these particles indicate that the particles mainly contain Fe elements and some Cr elements (Fig. 1d). The signal of the Cu element should come from the surrounding Cu matrix. Selected area electron diffraction (SAED) patterns are shown in Figs. 1e and 1f. When the electron beam is almost parallel with $[\bar{1}11]_{\text{Fe}}$, only a pair of spots of $\{200\}_{\text{Cu}}$ are observed. There is a misfit angle of 8° between $(200)_{\text{Cu}}$ and $(110)_{\text{Fe}}$. When the electron beam is almost parallel with $[011]_{\text{Cu}}$, only a pair of spots of $\{110\}_{\text{Fe}}$ are observed and are nearly parallel with the $\{220\}_{\text{Cu}}$. In a word, the SAED investigation indicates that there should be no special orientation relationship between the Cu matrix and Fe particles in either Cu-2.5% Fe-0.2% Cr or Cu-6% Fe alloys.

After heavy drawing, the original equal-axial Cu grains in the Cu-6% Fe alloy were elongated along the drawing direction (Fig. 2a). The Fe primary particles were also elongated and evolved into parallel Fe ribbons. At the transversal section of the drawn specimens, the Fe ribbons exhibit a curved morphology with an average thickness of 68.4 nm (Fig. 2b). The formation of the curved ribbon-like

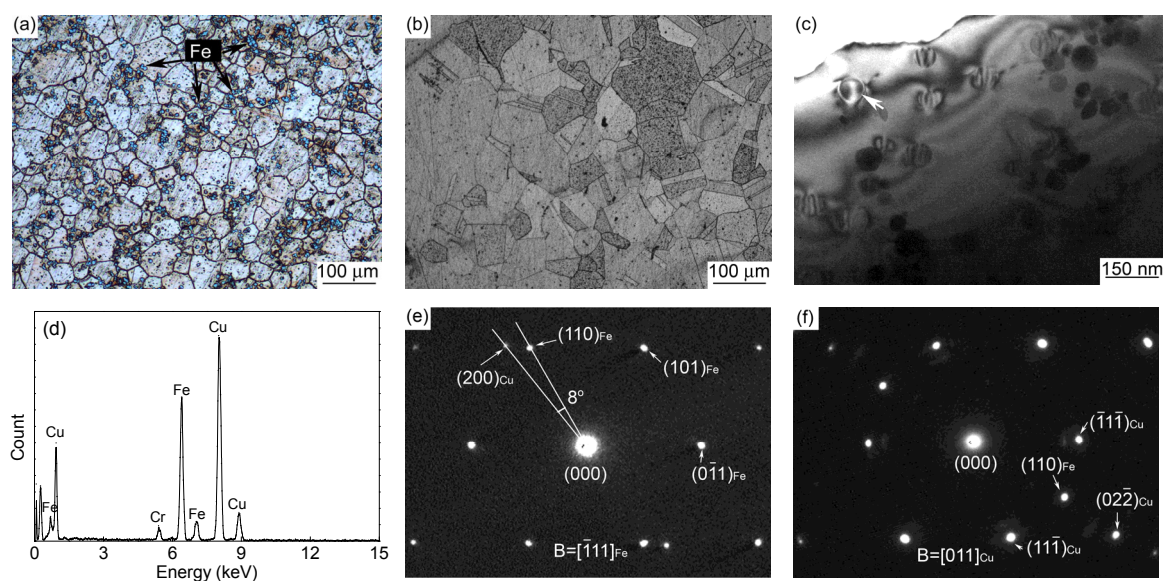


Fig. 1 Optical images of solution treated Cu-6% Fe (a) and aged Cu-2.5% Fe-0.2% Cr (b), TEM image of aged Cu-2.5% Fe-0.2% Cr (c), EDS spectra of a precipitate particle pointed by white arrow in Fig. 1c (d), and SAED patterns of Cu matrix and Fe particles when the electron beam is almost parallel with $[\bar{1}11]_{\text{Fe}}$ (e) and $[011]_{\text{Cu}}$ (f)

morphology has been widely observed in Cu-Fe and Cu-Nb alloys (Spitzig *et al.*, 1987; Biselli and Morris, 1996; Liu *et al.*, 2013; Deng *et al.*, 2014). The composites were reported to be highly textured: Nb had a $\langle 110 \rangle$ orientation whereas Cu had $\langle 111 \rangle$ and $\langle 100 \rangle$ textures (Raabe *et al.*, 1992; 1995a). The reason was fully explained that the BCC phase was forced to curl and fold due to the constraint of the surrounding FCC matrix, which is able to accommodate axially symmetric flow (Bevk *et al.*, 1978). The microstructure of the Cu-2.5% Fe-0.2% Cr alloy on the longitudinal section is similar to that of the Cu-6% Fe alloy, while there are only Cu filaments in the Cu-2.5% Fe-0.2% Cr alloy (Fig. 2c). High density of dislocation was observed inside the Cu filaments. Further investigation of the zone with high density of dislocation found many dislocations surrounding the Fe precipitate particles (Fig. 2d). The Fe precipitate particles still keep most of their spherical morphology, which indicates that they undergo little deformation during the drawing. The average diameter of the Fe precipitate particles is 62.2 nm in the Cu-2.5% Fe-0.2% Cr alloy at $\eta=6$, which is almost the same with that in the aged Cu-2.5% Fe-0.2% Cr alloy. High resolution transmission electron microscopy (HRTEM) investigation was employed to analyze the interface structure between the Cu

matrix and Fe particles. When the electron beam is almost parallel with $[100]_{\text{Fe}}$, no low-index of Cu matrix is parallel with the electron beam. Both planes of $(110)_{\text{Fe}}$ and $(1\bar{1}0)_{\text{Fe}}$ are clearly observed while nearly no lattice plane of the Cu matrix is visible as shown in Fig. 2e. When the electron beam is almost parallel with $[011]_{\text{Cu}}$, both planes of $(11\bar{1})_{\text{Cu}}$ and $(\bar{1}1\bar{1})_{\text{Cu}}$ are clearly observed as shown in Fig. 2f. At the same time, the planes of $(110)_{\text{Fe}}$ are visible but are not parallel with neither $(11\bar{1})_{\text{Cu}}$ nor $(\bar{1}1\bar{1})_{\text{Cu}}$. The HRTEM investigation indicates that there should be no special orientation relationship between Fe precipitate particles and the Cu matrix, which agrees very well with the results of the SAED patterns. The interface structure of Fe precipitate particles and the Cu matrix also shows typical incoherent phase interface characteristics.

Fig. 3 gives the mechanical and electrical properties of Cu-2.5% Fe-0.2% Cr and Cu-6% Fe alloys at various drawing strains. For comparison, the properties of pure Cu are also given in Fig. 3. The strength of the tested alloys increases with the increasing drawing strain. The strength increasing rates of Cu-2.5% Fe-0.2% Cr and Cu-6% Fe alloys are higher than that of pure Cu. The electrical resistivity of the tested alloys changes slightly with the

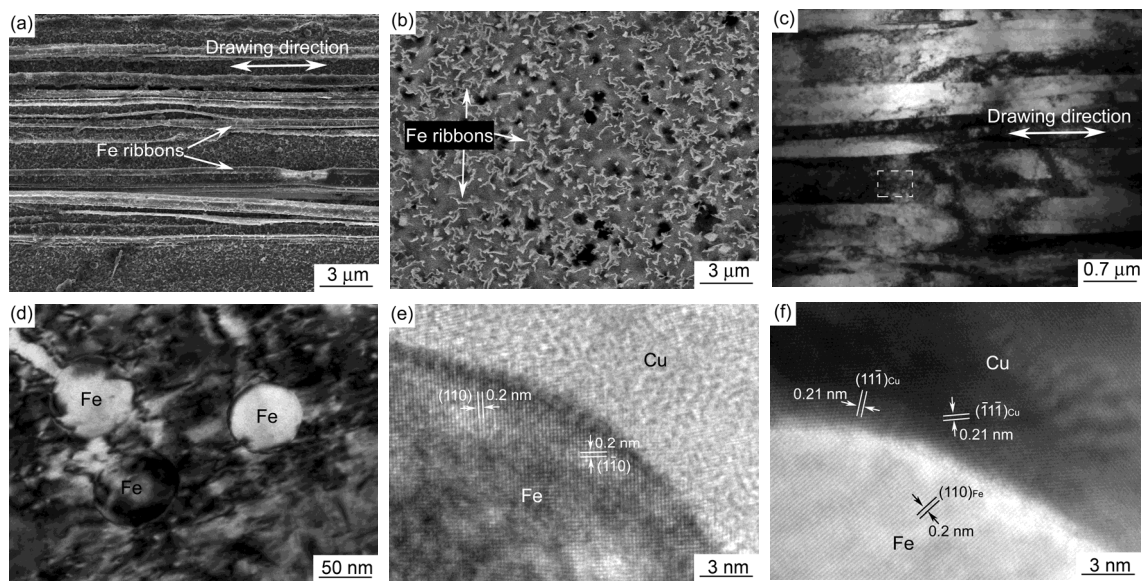


Fig. 2 SEM images of Cu-6% Fe at $\eta=6$ longitudinal section (a) and transversal section (b), TEM images of Cu-2.5% Fe-0.2% Cr at $\eta=6$ low magnification of longitudinal section (c) and high magnification of Fe precipitate particles in the white rectangle in Fig. 2c (d), and HRTEM images of a Fe precipitate particle embedded in Cu matrix when the electron beam is almost parallel with $[100]_{\text{Fe}}$ (e) and $[011]_{\text{Cu}}$ (f)

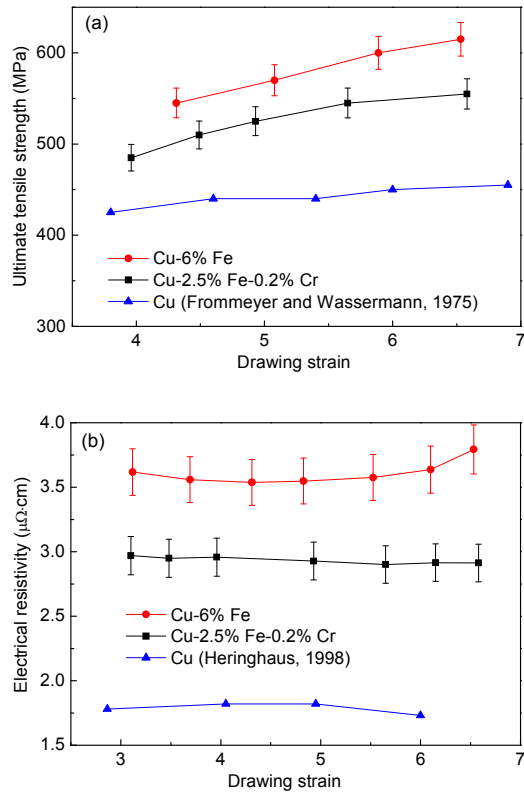


Fig. 3 Ultimate tensile strength (a) and electrical resistivity (b) of Cu-2.5% Fe-0.2% Cr, Cu-6% Fe, and pure Cu (Frommeyer and Wassermann, 1975; Heringhaus, 1998) dependent on the drawing strain

increasing drawing strain. The electrical resistivity of Cu-2.5% Fe-0.2% Cr and Cu-6% Fe alloys are obviously higher than that of pure Cu.

4 Discussion

Fe primary particles with a size of several micrometers were drawn into nano-ribbons by heavy drawing. However, Fe precipitate particles with a size of tens of nanometers were hardly deformed. Size effect should play a major role in different deformation behaviors of Fe primary particles and Fe precipitate particles. Studies on mechanical property of small size samples suggest that the flow stress of the samples increases with the size decreasing, following a Hall-Petch like equation (Hangen and Raabe, 1995; Legros *et al.*, 2000):

$$\sigma = \sigma_0 + kd^{-n}, \quad (1)$$

where σ and σ_0 are the flow stress and the lattice friction stress, respectively, d is the size of the sample, k is constant, and $n=0.5-1.0$. Dunstan and Bushby (2013) indicated that the strength should be inversely proportional to the size of the samples, and suggested that this effect could be explained by the room of the sample to activate the dislocation source. Namely, the smaller sample is stronger due to its harder activation of the dislocation source. According to these results, the deformation of Fe precipitate particles in Cu-2.5% Fe-0.2% Cr alloy should be much harder than Fe primary particles in Cu-6% Fe alloy.

Since Fe primary particles or Fe precipitate particles in tested alloys are embedded in the Cu matrix, taking into account the interaction between Cu and Fe phases during cold drawing, the plastic deformation behavior should be more complex. Studies of Cu-Ag alloys reveal that Ag precipitates produced by aging treatment are rod-like and are dozens of nanometers in diameter (Liu *et al.*, 2011b; Sitarama Raju *et al.*, 2013). These nano-scaled Ag precipitates could be evolved into extreme fine nanofibers by cold drawing. However, the nano-scaled Fe precipitate particles kept almost spherical morphology and underwent little deformation in this study. The main reason may lie in the different dislocation slip situations between Cu-Ag and Cu-Fe systems. For the Cu matrix and Ag precipitates, it has been confirmed that Ag precipitates have a cube-on-cube orientation relationship with the Cu matrix, that is $\langle 110 \rangle_{\text{Ag}} // \langle 110 \rangle_{\text{Cu}}$ and $\{111\}_{\text{Ag}} // \{111\}_{\text{Cu}}$ (Han *et al.*, 2003; Tian and Zhang, 2009). This orientation relationship can be well maintained even when the Cu-Ag alloys are heavily cold drawn (Liu *et al.*, 2011b). The cube-on-cube orientation relationship could guarantee Ag precipitates have the same dislocation slip system with the Cu matrix, which produces a greater benefit for the co-deformation of both phases. For the Cu matrix and Fe precipitate particles, the Fe precipitate particles are spherical and have no special orientation relationship. Little or even no favorite slip system of the Cu matrix is parallel with that of the Fe precipitate particles, which provides little help for the deformation of the Fe precipitate particles.

The evolution of Fe primary particles into Fe ribbons greatly increases the density of the Cu/Fe phase interface, which should be beneficial for the

strength of the Cu-6% Fe alloy. It has been documented that the phase interface plays a major strengthening role in the heavily drawn Cu- X (X =Nb, Fe, Ag, Cr) alloys (Biselli and Morris, 1996; Wu *et al.*, 2009; Badinier *et al.*, 2014). As a result, the Cu-6% Fe alloy shows a much higher strength than pure Cu. The strengthening situation in the Cu-2.5% Fe-0.2% Cr is notably different with that in Cu-6% Fe. Since the Fe precipitate particles are hardly deformed, the strengthening effect mainly results from the precipitation hardening by the well-known Orowan mechanism.

The resistivity of composites can be partitioned into the contribution of four scattering mechanisms: photon scattering, dislocation scattering, interface scattering, and impurity scattering (Raabe *et al.*, 1995b; Hong and Hill, 1999). The photon scattering component can be ignored at room temperature. The impurity scattering component is proportional to the impurity concentration, which is almost constant during the drawing process. The contribution from the dislocation scattering component is about $0.2 \mu\Omega\cdot\text{cm}$, which is relatively low (Karasek and Bevk, 1981). Therefore, the interface scattering component plays a main role. The density of the Cu/Fe phase interface in the Cu-6% Fe alloy increases with the increase of the drawing strain, which should enhance the electron scattering in the Cu-6% Fe alloy. As a result, the electrical resistivity of the Cu-6% Fe alloy slightly increases at $\eta < 6$ and greatly enhances at $\eta > 6$ at which stage the Fe particles are fully evolved into ribbons. However, the electrical resistivity of the Cu-2.5% Fe-0.2% Cr alloy keeps almost constant even at high drawing strains. Since the Fe precipitate particles are hardly deformed, the density of the Cu/Fe phase interface should be kept nearly constant, and therefore the electrical resistivity has little change.

5 Conclusions

Cu-2.5% Fe-0.2% Cr and Cu-6% Fe alloys were designed to compare the deformation behavior of the Fe phase with different scales. Fe primary particles with a size of about $5 \mu\text{m}$ were produced in the Cu-6% Fe alloy by solution treatment. Fe precipitate particles with a size of about 50 nm were produced

in the Cu-2.5% Fe-0.2% Cr alloy by a solution and aging treatment. During the cold drawing, Fe primary particles were elongated and evolved into nano-scaled ribbons. The density of the Cu/Fe phase interface gradually increases with the drawing strain. As a result, the strength and the electrical resistivity of the Cu-6% Fe alloy also increase with the drawing strain. In contrast, the Fe precipitate particles were hardly deformed and kept their spherical morphology even at $\eta=6$. High density of dislocation surrounds the Fe precipitate particles. The strength of the Cu-2.5% Fe-0.2% Cr alloy increases with the increase of the drawing strain and can be described by the Orowan mechanism. The electrical resistivity of the Cu-2.5% Fe-0.2% Cr alloy keeps almost constant since the density of the Cu/Fe phase interface shows hardly any change during cold drawing. The size effect and the incoherent interface of the Fe precipitate particles and Cu matrix play primary roles in the unchanging of Fe precipitate particles during cold drawing.

References

- Badinier, G., Sinclair, C.W., Allain, S., *et al.*, 2014. The Bauschinger effect in drawn and annealed nanocomposite Cu-Nb wires. *Materials Science and Engineering: A*, **597**:10-19. [doi:10.1016/j.msea.2013.12.031]
- Bevk, J., Harbison, J.P., Bell, J.L., 1978. Anomalous increase in strength of in situ formed Cu-Nb multifilamentary composites. *Journal of Applied Physics*, **49**(12):6031-6038. [doi:10.1063/1.324573]
- Biselli, C., Morris, D.G., 1994. Microstructure and strength of Cu-Fe in-situ composites obtained from prealloyed Cu-Fe powders. *Acta Metallurgica et Materialia*, **42**(1):163-176. [doi:10.1016/0956-7151(94)90059-0]
- Biselli, C., Morris, D.G., 1996. Microstructure and strength of Cu-Fe in situ composites after very high drawing strains. *Acta Materialia*, **44**(2):493-504. [doi:10.1016/1359-6454(95)00212-X]
- Deng, L.P., Han, K., Hartwig, K.T., *et al.*, 2014. Hardness, electrical resistivity, and modeling of *in situ* Cu-Nb microcomposites. *Journal of Alloys and Compounds*, **602**:331-338. [doi:10.1016/j.jallcom.2014.03.021]
- Dunstan, D.J., Bushby, A.J., 2013. The scaling exponent in the size effect of small scale plastic deformation. *International Journal of Plasticity*, **40**:152-162. [doi:10.1016/j.ijplas.2012.08.002]
- Frommeyer, G., Wassermann, G., 1975. Microstructure and anomalous mechanical properties of *in situ*-produced silver-copper composite wires. *Acta Metallurgica*, **23**(11):1353-1360. [doi:10.1016/0001-6160(75)90144-3]
- Han, K., Vasquez, A.A., Xin, Y., *et al.*, 2003. Microstructure and tensile properties of nanostructured Cu-25wt%Ag.

- Acta Materialia*, **51**(3):767-780. [doi:10.1016/S1359-6454(02)00468-8]
- Hangen, U., Raabe, D., 1995. Modeling of the yield strength of a heavily wire drawn Cu-20-percent-Nb composite by use of a modified linear rule of mixtures. *Acta Metallurgica et Materialia*, **43**(11):4075-4082. [doi:10.1016/0956-7151(95)00079-B]
- Heringhaus, F., 1998. Quantitative Analysis of the Influence of the Microstructure on Strength, Resistivity, and Magnetoresistance of Eutectic Silver-copper. PhD Thesis, Institut für Metallkunde und Metallphysik, RWTH Aachen, Germany; National High Magnetic Field Laboratory Tallahassee, USA.
- Hong, S.I., Hill, M.A., 1999. Mechanical stability and electrical conductivity of Cu-Ag filamentary microcomposites. *Materials Science and Engineering: A*, **264**(1-2):151-158. [doi:10.1016/S0921-5093(98)01097-1]
- Hong, S.I., Song, J.S., 2001. Strength and conductivity of Cu-9Fe-1.2X (X=Ag or Cr) filamentary microcomposite wires. *Metallurgical and Materials Transaction A*, **32**(4):985-991. [doi:10.1007/s11661-001-0356-7]
- Jia, N., Roters, F., Eisenlohr, P., et al., 2013. Simulation of shear banding in heterophase co-deformation: example of plane strain compressed Cu-Ag and Cu-Nb metal matrix composites. *Acta Materialia*, **61**(12):4591-4606. [doi:10.1016/j.actamat.2013.04.029]
- Karasek, K.R., Bevk, J., 1981. Normal-state resistivity of *in situ*-formed ultrafine filamentary Cu-Nb composites. *Journal of Applied Physics*, **52**(3):1370-1375. [doi:10.1063/1.329767]
- Legros, M., Elliott, B.R., Rittner, M.N., et al., 2000. Microsample tensile testing of nanocrystalline metals. *Philosophical Magazine A: Physics of Condensed Matter, Structure, Defects and Mechanical Properties*, **80**(4):1017-1026. [doi:10.1080/01418610008212096]
- Liu, J.B., Zhang, L., Meng, L., 2011a. Codeformation in Cu-6wt.% Ag nanocomposites. *Scripta Materialia*, **64**(7):665-668. [doi:10.1016/j.scriptamat.2010.12.015]
- Liu, J.B., Zhang, L., Yao, D.W., et al., 2011b. Microstructure evolution of Cu/Ag interface in the Cu-6 wt.% Ag filamentary nanocomposite. *Acta Materialia*, **59**(3):1191-1197. [doi:10.1016/j.actamat.2010.10.052]
- Liu, K.M., Lu, D.P., Zhou, H.T., et al., 2013. Influence of a high magnetic field on the microstructure and properties of a Cu-Fe-Ag *in situ* composite. *Materials Science and Engineering: A*, **584**:114-120. [doi:10.1016/j.msea.2013.07.016]
- Lu, X.P., Yao, D.W., Chen, Y., et al., 2014. Microstructure and hardness of Cu-12% Fe composite at different drawing strains. *Journal of Zhejiang University-SCIENCE A (Applied Physics & Engineering)*, **15**(2):149-156. [doi:10.1631/jzus.A1300164]
- Mattissen, D., Rabbe, D., Heringhaus, F., 1999. Experimental investigation and modeling of the influence of microstructure on the resistive conductivity of a Cu-Ag-Nb *in situ* composite. *Acta Materialia*, **47**(5):1627-1634. [doi:10.1016/S1359-6454(99)00026-9]
- Monzen, R., Kita, K., 2002. Ostwald ripening of spherical Fe particles in Cu-Fe alloys. *Philosophical Magazine Letters*, **82**(7):373-382. [doi:10.1080/09500830210137399]
- Pantsymy, V.I., Khlebova, N.E., Sudyev, S.V., et al., 2014. Thermal stability of the high strength high conductivity Cu-Nb, Cu-V, and Cu-Fe nanostructured microcomposite wires. *IEEE Transaction of Applied Superconductor*, **24**(3):0502804.
- Raabe, D., Ball, J., Gottstein, G., 1992. Rolling textures of a Cu-20-percent-Nb composite. *Scripta Metallurgica et Materialia*, **27**(2):211-216. [doi:10.1016/0956-716X(92)90115-U]
- Raabe, D., Heringhaus, F., Hangen, U., et al., 1995a. Investigation of a Cu-20 mass-percent Nb *in-situ* composite. 1. Fabrication, microstructure and mechanical properties. *Zeitschrift Fur Metallkunde*, **86**:405-415.
- Raabe, D., Heringhaus, F., Hangen, U., et al., 1995b. Investigation of a Cu-20 mass-percent Nb *in-situ* composite. 2. Electromagnetic properties and application. *Zeitschrift Fur Metallkunde*, **86**:416-422.
- Raabe, D., Miyake, K., Takahara, H., 2000. Processing, microstructure, and properties of ternary high-strength Cu-Cr-Ag *in situ* composites. *Materials Science and Engineering: A*, **291**(1-2):186-197. [doi:10.1016/S0921-5093(00)00981-3]
- Raju, K.S., Sarma, V.S., Kauffmann, A., et al., 2013. High strength and ductile ultrafine-grained Cu-Ag alloy through bimodal grain size, dislocation density and solute distribution. *Acta Materialia*, **61**(1):228-238. [doi:10.1016/j.actamat.2012.09.053]
- Sinclair, C.W., Embury, J.D., Weatherly, G.C., 1999. Basic aspects of the co-deformation of bcc/fcc materials. *Materials Science and Engineering: A*, **272**(1):90-98. [doi:10.1016/S0921-5093(99)00477-3]
- Sitarama Raju, K., Subramanya Sarma, V., Kauffmann, A., et al., 2013. High strength and ductile ultrafine-grained Cu-Ag alloy through bimodal grain size, dislocation density and solute distribution. *Acta Materialia*, **61**(1):228-238. [doi:10.1016/j.actamat.2012.09.053]
- Song, J.S., Hong, S.I., Kim, H.S., 2001. Heavily drawn Cu-Fe-Ag and Cu-Fe-Cr microcomposites. *Journal of Materials Processing Technology*, **113**(1-3):610-616. [doi:10.1016/S0924-0136(01)00665-3]
- Spitzig, W.A., Pelton, A.R., Laabs, F.C., 1987. Characterization of the strength and microstructure of heavily cold worked Cu-Nb composites. *Acta Metallurgica*, **35**(10):2427-2442. [doi:10.1016/0001-6160(87)90140-4]
- Tian, Y.Z., Zhang, Z.F., 2009. Microstructures and tensile deformation behavior of Cu-16wt.%Ag binary alloy. *Materials Science and Engineering: A*, **508**(1-2):209-213. [doi:10.1016/j.msea.2008.12.050]
- Tian, Y.Z., Wu, S.D., Zhang, Z.F., et al., 2011. Comparison of microstructures and mechanical properties of a Cu-Ag alloy processed using different severe plastic deformation modes. *Materials Science and Engineering: A*,

- 528(13-14):4331-4336. [doi:10.1016/j.msea.2011.01.057]
- Wang, Y.F., Gao, H.Y., Wang, J., et al., 2014. First-principles calculations of Ag addition on the diffusion mechanisms of Cu-Fe alloys. *Solid State Communications*, **183**:60-63. [doi:10.1016/j.ssc.2013.11.025]
- Watanabe, D., Watanabe, C., Monzen, R., 2008. Effect of coherency on coarsening of second-phase precipitates in Cu-base alloys. *Journal of Materials Science*, **43**(11): 3946-3953. [doi:10.1007/s10853-007-2373-4]
- Wu, Z.W., Chen, Y., Meng, L., 2009. Microstructure and properties of Cu-Fe microcomposites with prior homogenizing treatments. *Journal of Alloys and Compounds*, **481**(1-2):236-240. [doi:10.1016/j.jallcom.2009.03.078]
- Xie, Z., Gao, H., Wang, J., et al., 2011. Effect of homogenization treatment on microstructure and properties for Cu-Fe-Ag in situ composites. *Materials Science and Engineering: A*, **529**:388-392. [doi:10.1016/j.msea.2011.09.047]

中文概要

- 题目:** 冷拉拔 Cu-2.5% Fe-0.2% Cr 和 Cu-6% Fe 合金的显微组织与性能
- 目的:** 探索 Cu-Fe 合金中纳米尺寸和微米尺寸的 Fe 相的变形行为及区别。

方法: 1. 通过热处理在 Cu-2.5% Fe-0.2% Cr 合金中得到纳米级的 Fe 析出相, 在 Cu-6% Fe 中得到微米级的 Fe 析出相; 2. 通过冷拉拔手段使铜合金从棒状逐步变形成线材; 3. 使用光学显微镜、扫描电镜和透射电镜观察微观组织, 并用万能电子试验机测量抗拉强度, 用标准四点法测量电阻率。

结论: 1. 通过热处理在 Cu-6% Fe 合金中得到尺寸约 5 μm 的初生 Fe 颗粒, 在 Cu-2.5% Fe-0.2% Cr 合金中得到尺寸约 50 nm 的次生 Fe 颗粒; 2. 初生 Fe 颗粒在冷拉拔过程中转变成丝带状纤维, Cu/Fe 相界面密度随变形量增加而增加, 从而使 Cu-6% Fe 合金的强度和电阻率都随之增大; 3. 次生 Fe 颗粒即使在 $n=6$ 的时候也难以变形, 保持着球形的形貌, 同时高密度的位错环绕着 Fe 颗粒; Cu-2.5% Fe-0.2% Cr 合金的强度随变形量增加而增大, 遵循 Orowan 强化机制; Cu-2.5% Fe-0.2% Cr 合金的电阻率几乎保持不变, 因为 Cu/Fe 相界面密度在冷拉拔过程中几乎不变; 4. 尺寸效应和 Fe 析出颗粒与 Cu 基体的非共格界面对 Fe 析出颗粒在冷拉拔过程中不变形起到重要作用。

关键词: 铜合金; 变形; 显微组织; 强度